

# Phase Doubling and Entanglement in Coherent Many-Body Chemical Reactions

Shu Nagata<sup>1</sup>, Tadej Mežnaršič<sup>1</sup>, Chuixin Kong<sup>1</sup>, and Cheng Chin<sup>1</sup>  
<sup>1</sup>*James Franck Institute, Enrico Fermi Institute and Department of Physics,  
University of Chicago, Chicago, Illinois 60637, USA*

In the quantum degenerate regime, atoms and molecules can occupy a single quantum state, forming coherent matter waves. Here reactions are described by nonlinear mixing of the matter waves, giving rise to quantum many-body chemistry, where spatial coherence is preserved between the reactants and products. While the phase matching of matter waves during the reaction process has been theoretically predicted, experimental confirmation has remained elusive. Here we report on the observation of matter wave phase doubling when bosonic atoms pair into molecules. Using matter wave diffraction, we verify spatial phase coherence and observe a two-fold increase of phase in the molecular wavefunction, confirming the matter-wave version of phase doubling. The diffraction patterns also reveal non-classical correlations indicative of entangled atom pairs formed during the reaction. Our results establish molecular matter-wave diffraction as a powerful tool to probe quantum coherence and entanglement generation in chemically reactive quantum gases.

The wave-like behavior of massive particles, predicted by Louis de Broglie in 1924 [1], is one of the foundational principles of quantum mechanics. This concept of matter waves in which particles exhibit coherent wave-like properties has shaped our understanding of the microscopic world and continues to advance quantum technologies.

The wave-like nature of matter was first experimentally confirmed with electrons [2], followed by observations with atoms and molecules [3], and neutrons [4]. Recent diffraction experiments with large molecules [5] are pushing the limits of our knowledge of the quantum to classical boundary. Continued interest in research on matter waves has also led to the development of modern precision instruments, including electron microscopes [6], neutron [7] and atom interferometers [8], and quantum sensors [9, 10].

With the advent of advanced cooling and trapping techniques [11], long coherence times [12–14] and entanglement [15–17] have been observed in cold molecules, introducing a powerful platform to manipulate molecular ensembles for quantum information processing [18], matter wave interferometry [19] and controlled quantum chemistry [20–25].

An intriguing recent development is the formation of Bose-Einstein condensates (BECs) composed of short range molecules [26, 27]. Here, macroscopic numbers of molecules form a coherent matter wave. Theoretical studies suggest that chemical reactions in the quantum degenerate regime, described by nonlinear field mixing [28, 29], are phase coherent and can be Bose-enhanced, a phenomenon termed “quantum superchemistry” [30]. Bose-enhanced reactions have been observed in atom-molecule BECs [31].

To illustrate reactions in the quantum gas as a nonlinear field mixing process, we consider the synthesis of molecules in a single quantum state  $\psi_m$  from the pairing of atoms in a state  $\psi_a$ . This reaction is the matter wave analogue of second harmonic generation in nonlinear optics, where two red photons with frequency  $\omega_r$  are converted into a blue photon with frequency  $\omega_b = 2\omega_r$ . The interaction Hamiltonians for photons and atoms are

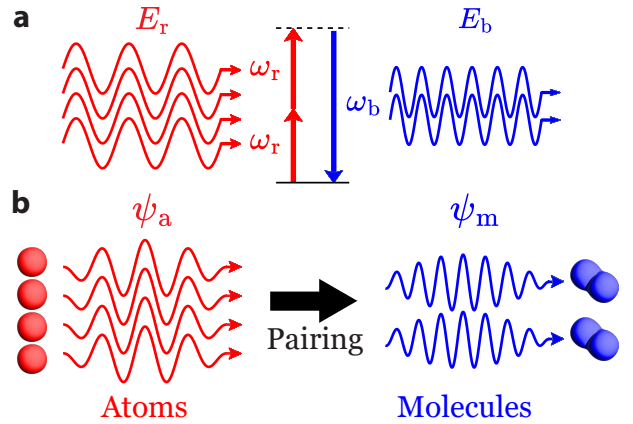


**FIG. 1. Pairing atoms into molecules: matter wave analogue of second harmonic generation in nonlinear optics.** **a**, Phase doubling in a nonlinear crystal, where pairs of red photons with frequency  $\omega_r$  are converted into blue photons with frequency  $\omega_b = 2\omega_r$ . **b**, In the matter wave analogue, atoms (red spheres) with wave function  $\psi_a$  are converted into diatomic molecules (blue spheres) with wave function  $\psi_m$ . Phase matching and entanglement generation are key features in the nonlinear wave mixing process.

both described by the nonlinear mixing of their corresponding fields

$$\begin{aligned} \text{Photon up/down conversion:} & \quad \chi \hat{E}_b^\dagger \hat{E}_r^2 + \chi \hat{E}_r^{\dagger 2} \hat{E}_b \\ \text{Atom + atom} \rightleftharpoons \text{molecule:} & \quad \gamma \hat{\psi}_m^\dagger \hat{\psi}_a^2 + \gamma \hat{\psi}_a^{\dagger 2} \hat{\psi}_m, \end{aligned}$$

where the coupling constant  $\chi$  for photons is given by the second order susceptibility  $\chi^{(2)}$  [33], and the coupling constant  $\gamma$  for atoms can be induced by Feshbach resonances in cold collisions [34]. Here,  $\hat{E}_r$  and  $\hat{E}_b$  are the field operators of the red and blue photon fields, and  $\hat{\psi}_a$  and  $\hat{\psi}_m$  are the field operators of the atomic and molecular fields.

An essential characteristic of nonlinear wave mixing in quantum optics is the phase matching of photonic fields.

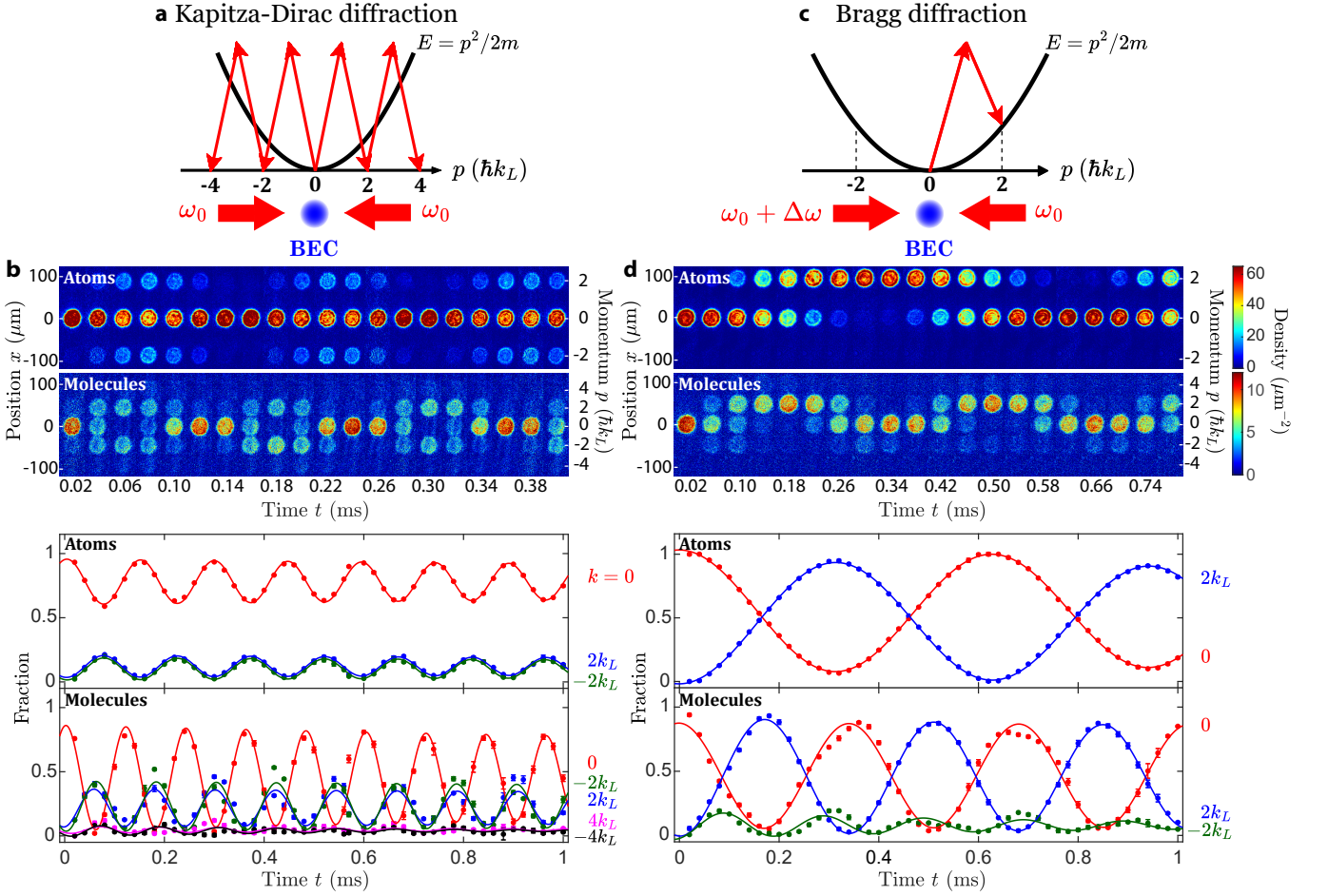


FIG. 2. **Kapitza-Dirac and Bragg diffraction of atomic and molecular BECs.** **a**, Kapitza-Dirac diffraction is induced by a pulse of counter-propagating laser beams at wavelength  $\lambda = 1064$  nm and identical frequencies  $\omega_0$  for a duration of time  $t$ . The optical lattice potential diffracts particles at zero momentum  $k = 0$  to  $\pm 2k_L, \pm 4k_L, \dots$ , where  $k_L = 2\pi/\lambda$  is the lattice momentum. **b**, Rabi oscillations of the atomic and molecular populations for Kapitza-Dirac diffraction. Images are taken after a 15 ms time-of-flight. The solid lines are sinusoidal fits which yield the Rabi frequencies  $2\pi \times 6.77(1)$  kHz for atoms and  $2\pi \times 8.31(1)$  kHz for molecules with momentum  $k = 0$  and  $\pm 2k_L$ . **c**, Bragg diffraction is realized by detuning one of the lattice beams by  $\Delta\omega = 4E_R/\hbar = 2\pi \times 5.304$  kHz for atoms and  $2E_R/\hbar = 2\pi \times 2.652$  kHz for molecules. The pulse resonantly scatters particles to momentum  $k = 2k_L$ . Here,  $E_R = \hbar^2 k_L^2 / 2m$  is the atomic recoil energy and  $m$  is the atomic mass. **d**, Rabi oscillations of the atomic and molecular populations for Bragg diffraction. The solid lines are sinusoidal fits which yield the Rabi frequency  $2\pi \times 1.59(1)$  kHz for atoms and  $2\pi \times 2.95(1)$  kHz for molecules. Decoherence rates of the observed oscillations are lower than  $0.2 \text{ ms}^{-1}$ . Off-resonant excitations to momentum  $k = -2k_L$  are stronger for molecules compared to atoms due to the larger Rabi coupling and smaller detuning [32]. Images shown here are averaged over five independent measurements. Error bars show  $1\text{-}\sigma$  standard deviations of the means.

Similarly, phase matching of matter wave fields is expected when atoms are paired into molecules. To see this, we note that the Hamiltonian is symmetric with respect to the gauge transformation  $\hat{\psi}_a \rightarrow \hat{\psi}_a e^{i\phi_a}$  and  $\hat{\psi}_m \rightarrow \hat{\psi}_m e^{2i\phi_a}$  [31]. Thus phase doubling  $\phi_m = 2\phi_a$  preserves the reaction dynamics. Describing the atomic and molecular fields as coherent matter waves  $\hat{\psi}_a = \sqrt{N}e^{i\phi_a}$  and  $\hat{\psi}_m = \sqrt{M}e^{i\phi_m}$ , where  $N(M)$  is the atom (molecule) number and  $\phi_a(\phi_m)$  is the atomic (molecular) phase, the phase difference (reaction phase)  $\phi_R \equiv 2\phi_a - \phi_m$  determines the direction of the chemical reaction, analogous to supercurrent in a Josephson junction [32]

$$\dot{M} = -\frac{\dot{N}}{2} = 2\gamma M N^2 \sin \phi_R.$$

When the atom and molecule populations reach an equilibrium  $\dot{M} = -\dot{N}/2 = 0$ , exact phase doubling is expected  $\phi_m = 2\phi_a$ .

Nonlinear field mixing is also a key process to generate entanglement between photons in quantum optics. Spontaneous parametric down conversion is a standard scheme to generate entangled photon pairs [35]. Continuous variable entanglement of twin beams is also routinely realized in optical parametric oscillators [36, 37]. There-

fore, entanglement generation is expected in the matter wave analogue where atomic and molecular fields are re-actively coupled [38].

In this paper, we report on phase doubling and entanglement generation when Bose-condensed atoms are paired into a molecular BEC. We first confirm the spatial coherence of the molecules based on matter wave diffraction. To demonstrate phase doubling, we imprint a phase pattern onto an atomic BEC with an optical standing wave pulse. After pairing the atoms into molecules, we extract the phase of the molecular BEC from its diffraction patterns and confirm the phase doubling during the reaction. We also evaluate the spin parity and entanglement witnesses from the diffraction patterns of the molecules, from which we conclude the non-separability and the nature of the entanglement of the molecular state.

Our experiment starts with a pure BEC of 120,000 cesium atoms prepared in a two-dimensional disk-shaped, flat-bottomed trap with a radius of 21  $\mu\text{m}$ . The atoms are strongly confined in the vertical direction to an optical dipole trap with trap frequency of  $\omega_z = 2\pi \times 590$  Hz. The condensate is prepared at a magnetic field of  $B = 20.25$  G with an atomic scattering length  $a = 180a_0$ , where  $a_0$  is the Bohr radius and the chemical potential is  $\mu = k_B \times 40$  nK [26].

To synthesize molecules, the magnetic field is ramped across a  $g$ -wave Feshbach resonance at 19.849 G, which converts the atomic BEC into a molecular BEC of up to 20,000 molecules [31]. The ramp is followed by a fast quench of the field to 17.2 G and then a resonant beam to remove any remaining atoms. To detect the molecules, we dissociate them into atoms by ramping the magnetic field above the resonance and image the atoms.

In our first experiment, we perform matter-wave diffraction on the atomic and molecular BECs to verify their spatial coherence. A one-dimensional optical lattice with period  $\lambda/2 = 532$  nm is applied on the sample, which diffracts the particles to discrete momentum modes  $k = \pm 2k_L, \pm 4k_L, \dots$ , where  $k_L = 2\pi/\lambda$  is the lattice wavenumber, see Fig. 2a. The diffracted particles are spatially separated from the BEC after time-of-flight expansion. We realize Kapitza-Dirac diffraction with a static lattice potential, which symmetrically scatters particles to positive and negative modes, see Figs. 2a, b, and Bragg diffraction with a moving lattice, which resonantly couples the BEC to the  $|2k_L\rangle$  state, see Figs. 2c, d. We note that the diffracted molecules move at half the speed of the atoms since they are twice as massive.

Both diffraction processes induce coherent population transfer of atoms and molecules between zero and finite momentum modes. We observe weak decoherence rates for both atoms and molecules, indicating that the coherence is preserved during the pairing process. The oscillation frequencies of the diffracted populations also provide precise information on the energy dispersion of the particles in the lattice potential. By comparing the measurements results to the band theory calculation, we

determine the molecular dynamical polarizability to be  $\alpha_m = k_B \times 5.05(5)$  nK  $\cdot$  cm<sup>2</sup>/W =  $1.95(2)\alpha_a$ , which is approximately twice the atomic polarizability  $\alpha_a$  [32].

Bragg diffraction is a powerful tool to probe the phase relationship of atomic and molecular matter waves. A short Bragg pulse on the atomic BEC can imprint a phase pattern  $\phi_a(x)$  on the wavefunction  $\psi_a(x) = \sqrt{n_a(x)}e^{i\phi_a(x)}$ . Following the pulse, we pair the atoms into molecules, and examine how the atomic phase transforms into phase  $\phi_m(x)$  of the molecular wavefunction  $\psi_m(x) = \sqrt{n_m(x)}e^{i\phi_m(x)}$ . Here  $n_a$  and  $n_m$  are the atomic and molecular densities. The scheme is illustrated in Fig. 3a.

The phase information of the atomic and molecular matter waves can be readily extracted from their diffraction patterns. To see this, we express a wavefunction  $\psi(x)$  as

$$\psi(x) = \sqrt{n(x)}e^{i\phi(x)} = \sum_{j=0,\pm 1,\pm 2,\dots} \psi_{2j}e^{2ijk_L x}, \quad (1)$$

where  $\psi_{2j}$  is the amplitude of the plane wave with momentum  $2jk_L$ . For Bragg-diffracted atoms, the single particle wavefunction  $\psi_a(x) = \cos(\Omega_a t/2) - i\sin(\Omega_a t/2)e^{2ik_L x}$  can be described by rotation of spins with Rabi frequency  $\Omega_a$ . From Eq. (1), the phase modulation evaluated at the anti-nodes of the lattice  $\phi_a$  is given by the spin rotation angle  $\phi_a = \Omega_a t/2$ , and can be extracted in our experiment from the atomic populations  $n_0 = \cos^2 \phi_a$  and  $n_2 = \sin^2 \phi_a$  based on

$$\cot^2 \phi_a = \frac{n_0}{n_2}. \quad (2)$$

The pairing of atoms in two momentum modes results in molecules occupying three modes described by the wavefunction  $\psi_m(x) = \psi_{m0} + \psi_{m2}e^{2ik_L x} + \psi_{m4}e^{4ik_L x}$ . Molecules with zero momentum  $k = 0$  and  $4k_L$  come from pairing atoms with the same momentum  $k = 0$  and  $2k_L$ , the matter-wave analogue of second harmonic generation (SHG). The molecular populations scale as  $m_0 \propto \gamma^2 n_0^2$  and  $m_4 \propto \gamma^2 n_2^2$ , where  $\gamma$  is the Feshbach coupling strength. Molecules with momentum  $k = 2k_L$  come from pairing atoms with distinct momenta  $k = 0$  and  $2k_L$ , the matter-wave analogue of sum frequency generation (SFG). The  $k = 2k_L$  population scales as  $m_2 \propto 4\gamma_2^2 n_0 n_2$ , where  $\gamma_2$  is the sum frequency coupling strength and the factor of 4 comes from bosonic symmetrization [32], see Fig. 3a.

We measure the molecular populations after time-of-flight expansion. The normalized populations  $m_0 = |\psi_{m0}|^2$  and  $m_4 = |\psi_{m4}|^2$  oscillate at the atomic Rabi frequency  $\Omega_a$ . They reach unity when atoms occupy a single momentum state after  $0, \pi, 2\pi, \dots$  Bragg pulses. On the other hand, the population  $m_2 = |\psi_{m2}|^2$  oscillates at twice the Rabi frequency  $2\Omega_a$  and reaches the maximum  $A_2 = 0.58(1)$  after  $\pi/2, 3\pi/2, \dots$  Bragg pulses on the atoms, see Figs. 3b and c.

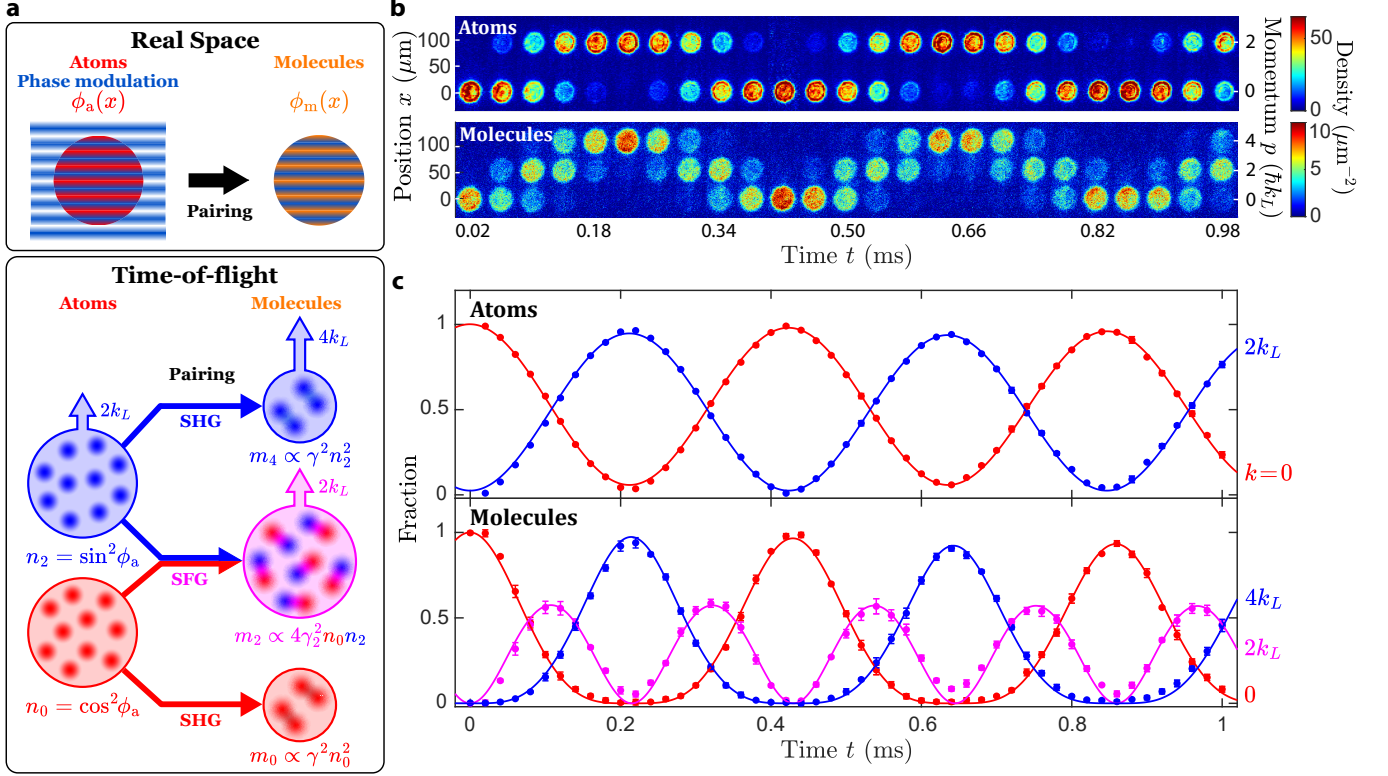


FIG. 3. **Phase modulation on atomic and molecular BECs.** **a**, Experimental protocol. A Bragg diffraction pulse imprints a phase  $\phi_a(x)$  onto the atomic BEC. The atomic BEC is then converted into a molecular BEC with phase  $\phi_m(x)$ . The imprinted phase is reflected in the populations of diffracted atoms,  $n_0 = \cos^2 \phi_a$  and  $n_2 = \sin^2 \phi_a$ . After pairing, molecules occupy momenta  $k = 0, 2k_L$  and  $4k_L$  with populations  $m_0, m_2$ , and  $m_4$ , which are proportional to the products of atomic populations. The populations of  $m_0$  and  $m_4$  are generated by second harmonic generation (SHG) with coupling constant  $\gamma$  while  $m_2$  is generated by sum frequency generation (SFG) with  $\gamma_2$ . The factor of 4 in  $m_2$  comes from bosonic exchange symmetry. **b**, Oscillations of momentum state populations as a result of phase modulation on the atomic and molecular BECs. Images are taken after 16 ms time-of-flight expansion. Images shown here are averaged over five independent measurements. **c**, Populations of diffracted atoms and molecules. Atomic populations oscillate at a Rabi frequency of  $\Omega_a = 2\pi \times 2.36(1)$  kHz. Molecular populations in momenta  $k = 0, 2k_L$ , and  $4k_L$  are fit to  $m_0 = \cos^4 \Omega_0 t/2$ ,  $m_2 = A_2 \sin^2 \Omega_2 t/2$  and  $m_4 = \sin^4 \Omega_4 t/2$ , which give  $\Omega_0 = 2\pi \times 2.33(1)$ ,  $\Omega_2 = 2\pi \times 4.66(1)$ , and  $\Omega_4 = 2\pi \times 2.33(1)$  kHz, respectively and  $A_2 = 0.58(1)$ . Error bars show 1- $\sigma$  standard deviations of the means.

The model accurately describes the measurement results, and we obtain the ratio of the coupling constants  $\gamma_2/\gamma = 0.82(3)$ . The smaller value of  $\gamma_2$  compared to  $\gamma$  is consistent with our expectation that the sum frequency coupling is off-resonant by two atomic recoil energies, resulting in a lower coupling efficiency [32].

The molecular diffraction pattern reveals the phase modulation of the molecular matter waves. Applying Eq. (1), we evaluate the amplitude of the phase modulation according to

$$\cot \phi_m = \frac{\sqrt{m_0} - \sqrt{m_4}}{\sqrt{m_2}}. \quad (3)$$

We compare the molecular phase  $\phi_m$  to the atomic phase  $\phi_a$ , see Fig. 4a. The molecular phase evolves twice as much as the atomic phase  $\phi_m = 2\phi_a$  over several Rabi cycles, confirming phase doubling during the synthesis of molecules.

A closer examination suggests a small nonlinear correction to the exact phase doubling. The correction comes from the imbalance of the SFG and SHG coupling strengths  $\gamma_2 \neq \gamma$ , and is predicted to be [32]

$$\phi_m - 2\phi_a = -\epsilon \sin 4\phi_a + \mathcal{O}(\epsilon^2), \quad (4)$$

where we obtain  $\epsilon = 0.06(2)$  from the fit to the data in Fig. 4a, which is in agreement with the theoretical value of  $\epsilon = \frac{1}{2}(1 - \gamma_2/\gamma) \approx 0.09(2)$ .

The phase doubling experiment also reveals entanglement generation during the formation of molecules. We start by testing the separability of atoms in the molecular state by evaluating the spin parity  $C_{zz} = \langle \hat{\sigma}_{1,z} \otimes \hat{\sigma}_{2,z} \rangle = m_0 - m_2 + m_4$ , where  $\hat{\sigma}_{j,z}$  is the Pauli-Z operator on the  $j$ -th atom [39]. For product states of two identical particles, the parity is constrained within  $0 \leq C_{zz} \leq 1$ . Negative parity  $-1 \leq C_{zz} < 0$  indicates the non-separability and entanglement of the atom pairs [32].



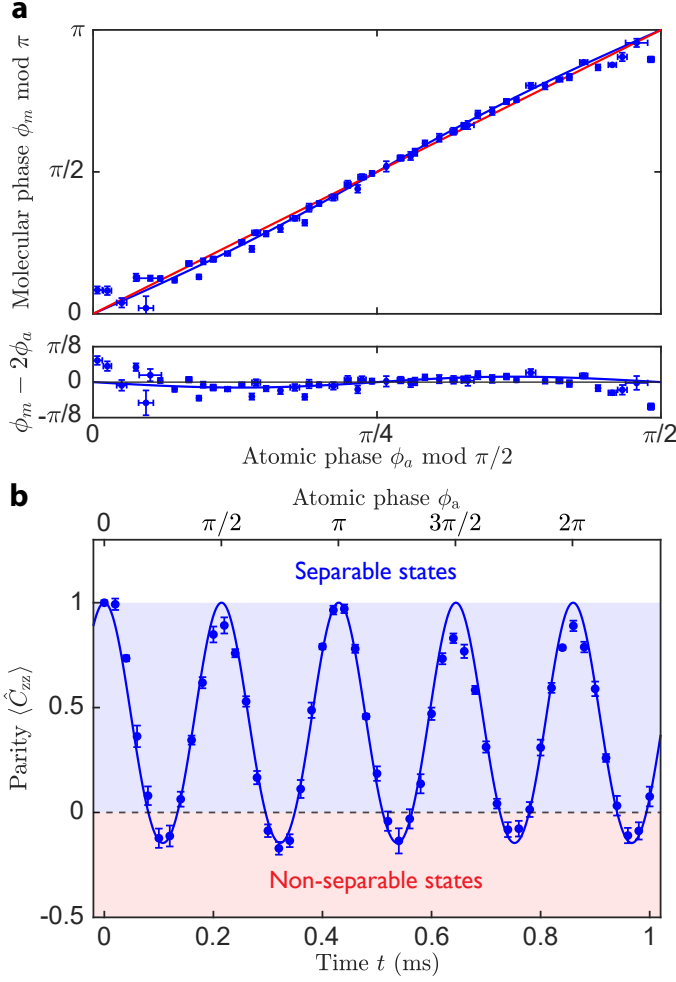


FIG. 4. **Matter wave phase doubling and entanglement generation.** **a**, Dependence of the molecular phase  $\phi_m$  on the atomic phase  $\phi_a$ . The phases  $\phi_a$  and  $\phi_m$  are extracted from the diffraction patterns shown in Fig. 3. The measurements (blue circles) are compared to the red line which represents a linear ratio of  $\phi_m/\phi_a = 2$ . The blue line is the fit to the theoretical model  $\phi_m = 2\phi_a - \epsilon \sin 4\phi_a$ . The lower panel shows the deviation of the data from the phase doubling ratio  $\phi_m = 2\phi_a$ . The residual is fit to  $-\epsilon \sin 4\phi_a$  (blue line), from which we obtain  $\epsilon = 0.06(2)$ . **b**, Spin parity  $\langle \hat{C}_{zz} \rangle = m_0 - m_2 + m_4$  for molecules. Negative parity  $-1 \leq \langle \hat{C}_{zz} \rangle < 0$  indicates non-separability of the two-atom quantum state. Error bars show 1- $\sigma$  standard deviation of the mean of 5 measurements.

In Fig. 4b, we show that the parity  $C_{zz}$  oscillates at twice the atomic Rabi frequency. The parity reaches the maximum of  $C_{zz} = 1$ , when the molecules are in a single momentum state  $|0\rangle$  or  $|4k_L\rangle$ . The parity reaches the minimum of  $C_{zz} = -0.15(1) < 0$  and enters the non-separable regime, when atoms are prepared in an equal superposition of  $|0\rangle$  and  $|2k_L\rangle$  after a  $\pi/2, 3\pi/2, \dots$  Bragg pulse. Here atoms in the molecular state exhibit the highest degree of entanglement.

To elucidate the nature of the entanglement, we compute the entanglement witnesses  $W_{\Psi^\pm}$  and  $W_{\Phi^\pm}$  of the molecular state after a  $\pi/2$ -pulse [32, 40]. The witnesses reflect overlap with the maximally entangled Bell states  $|\Psi^\pm\rangle = (|00\rangle \pm |11\rangle)/\sqrt{2}$  and  $|\Phi^\pm\rangle = (|01\rangle \pm |10\rangle)/\sqrt{2}$ . A positive value of  $W_{\Phi^+} = -2C_{zz} = 0.29(2)$  and negative values for all other witnesses indicates that the state resembles the Bell state  $|\Phi^+\rangle$ . From the witnesses, we reconstruct the molecular wavefunction after a  $\pi/2$ -pulse  $|\psi_m\rangle = \frac{1}{2}\sqrt{2 - W_{\Phi^+}}|\Psi^-\rangle - \frac{i}{2}\sqrt{2 + W_{\Phi^+}}|\Phi^+\rangle$ .

To understand the origin of the entanglement, we consider a constant Feshbach coupling strength  $\gamma_2 = \gamma$  for both SFG and SHG processes. In the momentum picture, the wave mixing Hamiltonian  $\hat{H} \propto (\hat{\psi}_{a0} + \hat{\psi}_{a2})^2$  generates constructive interference of the cross terms  $\hat{\psi}_{a0}\hat{\psi}_{a2} + \hat{\psi}_{a2}\hat{\psi}_{a0} = 2\hat{\psi}_{a2}\hat{\psi}_{a0}$ . Therefore, the sum frequency component  $m_2 \propto 4\langle \hat{\psi}_{a0}^\dagger \hat{\psi}_{a2}^\dagger \hat{\psi}_{a2} \hat{\psi}_{a0} \rangle$  is double the classical joint probability  $2\langle \hat{\psi}_{a0}^\dagger \hat{\psi}_{a0} \rangle \langle \hat{\psi}_{a2}^\dagger \hat{\psi}_{a2} \rangle$ , due to the nonlinearity of the pairing interaction. For sufficiently strong sum frequency production  $\gamma_2 > \gamma/\sqrt{2}$ , the molecular state is closer to  $|\Phi^+\rangle$  with  $W_{\Phi^+} = (2\gamma_2^2 - \gamma^2)/(\gamma_2^2 + \gamma^2/2) > 0$ .

Remarkably, the sum frequency generation  $m_2 \propto 4\langle \hat{\psi}_{a0}^\dagger \hat{\psi}_{a2}^\dagger \hat{\psi}_{a2} \hat{\psi}_{a0} \rangle = 4g^{(2)}\langle \hat{\psi}_{a0}^\dagger \hat{\psi}_{a0} \rangle \langle \hat{\psi}_{a2}^\dagger \hat{\psi}_{a2} \rangle$  depends on the second order correlation of the atoms  $g^{(2)}$  [32, 41], which is  $g^{(2)} \approx 1$  for our atomic BECs. The molecular populations can therefore serve as probes for the correlation of atomic samples (the matter-wave analogue of the Hanbury Brown and Twiss effect).

**Acknowledgement** We thank S. Cornish, X. Lai, and S. Mystakidis for helpful discussions. We thank Z. Yan and J. Jachinowski for carefully reading the manuscript. This work was supported by the National Science Foundation under Grant No. PHY1511696 and PHY-2103542, by the Air Force Office of Scientific Research under award number FA9550-21-1-0447. S. N. acknowledges support from the Takenaka Scholarship Foundation.

[1] Broglie, L. & Nishimura, H. *Research on the theory of quanta* (2021).  
[2] Davisson, C. & Germer, L. H. Diffraction of Electrons by a Crystal of Nickel. *Physical Review* **30**, 705–740 (1927).  
[3] Estermann, I. & Stern, O. Beugung von Molekularstrahlen. *Zeitschrift für Physik* **61**, 95–125 (1930).  
[4] H., V. H. Preuve Experimentale de la Diffraction des Neutrons. *Acad. Sci. Paris* **203**, 73–75 (1936).  
[5] Brand, C. *et al.* Bragg Diffraction of Large Organic

Molecules. *Physical Review Letters* **125**, 033604 (2020).  
[6] Egerton, R. *Physical Principles of Electron Microscopy* (Springer International Publishing, 2016).  
[7] Greenberger, D. M. The neutron interferometer as a device for illustrating the strange behavior of quantum systems. *Reviews of Modern Physics* **55**, 875–905 (1983).  
[8] Bongs, K. *et al.* Taking atom interferometric quantum sensors from the laboratory to real-world applications. *Nature Reviews Physics* **1**, 731–739 (2019).

- [9] Degen, C., Reinhard, F. & Cappellaro, P. Quantum sensing. *Reviews of Modern Physics* **89**, 035002 (2017).
- [10] Stray, B. *et al.* Quantum sensing for gravity cartography. *Nature* **602**, 590–594 (2022).
- [11] Langen, T., Valtolina, G., Wang, D. & Ye, J. Quantum state manipulation and cooling of ultracold molecules. *Nature Physics* **20**, 702–712 (2024).
- [12] Park, J. W., Yan, Z. Z., Loh, H., Will, S. A. & Zwierlein, M. W. Second-scale nuclear spin coherence time of ultracold  $^{23}\text{Na}^{40}\text{K}$  molecules. *Science* **357**, 372–375 (2017).
- [13] Zhou, Y. *et al.* Second-scale coherence measured at the quantum projection noise limit with hundreds of molecular ions. *Phys. Rev. Lett.* **124**, 053201 (2020).
- [14] Burchesky, S. *et al.* Rotational Coherence Times of Polar Molecules in Optical Tweezers. *Physical Review Letters* **127**, 123202 (2021).
- [15] Holland, C. M., Lu, Y. & Cheuk, L. W. On-demand entanglement of molecules in a reconfigurable optical tweezer array. *Science* **382**, 1143–1147 (2023).
- [16] Bao, Y. *et al.* Dipolar spin-exchange and entanglement between molecules in an optical tweezer array. *Science* **382**, 1138–1143 (2023).
- [17] Ruttley, D. K., Hepworth, T. R., Guttridge, A. & Cornish, S. L. Long-lived entanglement of molecules in magic-wavelength optical tweezers. *Nature* **637**, 827–832 (2025).
- [18] Cornish, S. L., Tarbutt, M. R. & Hazzard, K. R. A. Quantum computation and quantum simulation with ultracold molecules. *Nature Physics* **20**, 730–740 (2024).
- [19] Li, C., Liang, Q., Paranjape, P., Wu, R. & Schmiedmayer, J. Matter-wave interferometers with trapped strongly interacting Feshbach molecules. *Phys. Rev. Res.* **6**, 023217 (2024).
- [20] Bohn, J. L., Rey, A. M. & Ye, J. Cold molecules: Progress in quantum engineering of chemistry and quantum matter. *Science* **357**, 1002–1010 (2017).
- [21] Croft, J. F. E. *et al.* Universality and chaoticity in ultracold K+KRb chemical reactions. *Nature Communications* **8** (2017).
- [22] Hoffmann, D. K., Paintner, T., Limmer, W., Petrov, D. S. & Denschlag, J. H. Reaction kinetics of ultracold molecule-molecule collisions. *Nature Communications* **9** (2018).
- [23] Chen, X.-Y. *et al.* Ultracold field-linked tetratomic molecules. *Nature* **626**, 283–287 (2024).
- [24] Liu, Y.-X. *et al.* Quantum interference in atom-exchange reactions. *Science* **384**, 1117–1121 (2024).
- [25] Martins, F. B. V., Schmutz, H., Agner, J. A., Zhelyazkova, V. & Merkt, F. Microwave-Controlled Cold Chemistry. *Physical Review Letters* **134**, 123401 (2025).
- [26] Zhang, Z., Chen, L., Yao, K.-X. & Chin, C. Transition from an atomic to a molecular Bose–Einstein condensate. *Nature* **592**, 708–711 (2021).
- [27] Bigagli, N. *et al.* Observation of Bose–Einstein condensation of dipolar molecules. *Nature* **631**, 289–293 (2024).
- [28] Moore, M. G. & Vardi, A. Bose-Enhanced Chemistry: Amplification of Selectivity in the Dissociation of Molecular Bose-Einstein Condensates. *Phys. Rev. Lett.* **88**, 160402 (2002).
- [29] Malla, R. K., Chernyak, V. Y., Sun, C. & Sinitsyn, N. A. Coherent Reaction between Molecular and Atomic Bose–Einstein Condensates: Integrable Model. *Physical Review Letters* **129**, 033201 (2022).
- [30] Heinzen, D. J., Wynar, R., Drummond, P. D. & Kheruntsyan, K. V. Superchemistry: Dynamics of Coupled Atomic and Molecular Bose–Einstein Condensates. *Physical Review Letters* **84**, 5029–5033 (2000).
- [31] Zhang, Z., Nagata, S., Yao, K.-X. & Chin, C. Many-body chemical reactions in a quantum degenerate gas. *Nature Physics* **19**, 1466–1470 (2023).
- [32] See supplementary materials.
- [33] Agarwal, G. Quantum theory of second harmonic generation. *Optics Communications* **1**, 132–134 (1969).
- [34] Chin, C., Grimm, R., Julienne, P. & Tiesinga, E. Feshbach resonances in ultracold gases. *Reviews of Modern Physics* **82**, 1225–1286 (2010).
- [35] Anwar, A., Perumangatt, C., Steinlechner, F., Jennewein, T. & Ling, A. Entangled photon-pair sources based on three-wave mixing in bulk crystals. *Review of Scientific Instruments* **92** (2021).
- [36] Dell’Anno, F., De Siena, S. & Illuminati, F. Multiphoton quantum optics and quantum state engineering. *Physics Reports* **428**, 53–168 (2006).
- [37] Adesso, G. & Illuminati, F. Entanglement in continuous-variable systems: recent advances and current perspectives. *Journal of Physics A: Mathematical and Theoretical* **40**, 7821–7880 (2007).
- [38] Poulsen, U. V. & Mølmer, K. Quantum states of bose-einstein condensates formed by molecular dissociation. *Physical Review A* **63**, 023604 (2001).
- [39] Sackett, C. A. *et al.* Experimental entanglement of four particles. *Nature* **404**, 256–259 (2000).
- [40] Hyllus, P., Gühne, O., Bruß, D. & Lewenstein, M. Relations between entanglement witnesses and bell inequalities. *Physical Review A* **72**, 012321 (2005).
- [41] Meiser, D., Meystre, P. & Search, C. P. Molecule formation as a diagnostic tool for second-order correlations of ultracold gases. *Physical Review A* **71**, 033621 (2005).
- [42] Grimm, R., Weidemüller, M. & Ovchinnikov, Y. B. Optical Dipole Traps for Neutral Atoms. vol. 42 of *Advances In Atomic, Molecular, and Optical Physics*, 95–170 (Academic Press, 2000).
- [43] Rafac, R. J. & Tanner, C. E. Measurement of the ratio of the cesium *d*-line transition strengths. *Phys. Rev. A* **58**, 1087–1097 (1998).
- [44] Zhang, Z. *Coherent Dynamics and Reactions in Atomic and Molecular Bose-Einstein Condensates*. Ph.D. thesis, University of Chicago (2022).

## Supplementary Material

### I. METHODS

#### A. Preparation of atomic and molecular BECs

Our experiment starts with 120,000 Bose-condensed  $^{133}\text{Cs}$  atoms in a two-dimensional (2D) cylindrical flat-bottomed trap at magnetic field  $B \sim 20.3$  G. The atoms are polarized in the ground state  $|F = 3, m_F = 3\rangle$  where  $F$  and  $m_F$  are the quantum numbers for the total angular momentum and its projection along the direction of the magnetic field, respectively. The atoms are trapped by a blue-detuned ring-like barrier generated by a digital micromirror device (DMD) in the radial direction and an optical dipole trap with a trap frequency of  $\omega_z = 2\pi \times 590$  Hz in the vertical direction. To create molecules, we rapidly sweep the magnetic field across the narrow  $g$ -wave Feshbach resonance at 19.849 G with a width of 8.3 mG in 1.5 ms to couple the Cs atoms into  $\text{Cs}_2$  molecules in  $|f = 4, m_f = 4; l = 4, m_l = 2\rangle$  where  $f$  is the total angular momentum quantum number of the molecule and  $l$  is the molecular orbital angular momentum quantum number, and  $m_f$  and  $m_l$  are the projections of  $f$  and  $l$  along the direction of the magnetic field, respectively [26]. After the sweep, we jump the magnetic field far away from the resonance to 17.2 G and blow away any remaining atoms using a resonant light pulse. To image the molecules, we dissociate them back into atoms by sweeping across the Feshbach resonance again from 19.5 to 20.4 G in less than 1 ms and image the atoms using absorption imaging.

#### B. Optical lattice diffraction experiment

To diffract the particles, we apply a pulse of an optical standing wave from a Nd:YAG laser with wavelength  $\lambda = 1064$  nm. The standing wave is prepared by retro-reflecting the incident beam which passes through the sample and then a pair of acousto-optic modulators (AOMs) which we use to tune the frequency of the retro-reflected beam. For Kapitza-Dirac diffraction, we set the retro-reflected beam to have the same frequency as the incident beam to create a static lattice.

For Bragg diffraction, the retro-reflected beam is detuned by  $\Delta f = 5.304$  kHz and  $\Delta f = 2.652$  kHz for atoms and molecules, respectively, to resonantly transfer particles to momentum  $k = 2k_L$ . This is realized by setting the AOMs to  $+80$  MHz  $+\Delta f/2$  and  $-80$  MHz. The retro-reflected beam passes through the AOMs twice and acquires the desired detuning  $\Delta f$ .

To measure the atomic and molecular populations in different momentum modes, we perform a 2D time-of-flight (TOF) expansion to spatially separate atoms and molecules in different orders. We expand the sample in the radial  $x - y$  direction by shutting off the DMD potential barrier while keeping the dipole trap turned on in the  $z$ -direction such that the sample only expands radially. Before the lattice pulse, we quench the scattering length to  $0a_0$  for atoms. The scattering length of the molecules is fixed at  $220a_0$  [26].

After  $t = 15$  ms, when the different diffracted orders are sufficiently separated, we image the sample and determine the populations by counting the particle number in each momentum mode. The TOF is short enough such that the diffracted components maintain the disk-shape of the initial BEC. To obtain the precise particle number, we carefully evaluate and compensate for the background signal and integrate the particle numbers within the circular area of the BEC for each diffracted mode. This procedure allows us to determine the atomic and molecular populations shown in Figs. 2 and 3.

We use an empirical function to fit the atomic and molecular Rabi oscillations in Fig. 2

$$P(t) = P(0) \cos(\Omega t + \theta) e^{-\eta t} + c, \quad (\text{S1})$$

where  $P$  is the population,  $\theta$  is the phase shift,  $\eta$  is the decay rate and  $c$  is a constant. The results from the fitting are listed in Tables S1 and S2. From these measurement results, we determine the lattice potential depth to be  $4.70(2)$  and  $9.31(2)$   $E_R$  for atoms and molecules, respectively, in Fig. 2b for Kapitza-Dirac diffraction, and  $2.41(1)$  and  $4.83(1)$   $E_R$  for atoms and molecules, respectively, in Fig. 2d for Bragg diffraction. Since the lattice beam intensity is the same for both atoms and molecules, the different potential depths for atoms and molecules suggest a difference in their dynamical polarizabilities.

TABLE S1. Oscillation frequencies and decay rates of the Kapitza-Dirac diffracted atomic and molecular populations obtained from the fits in Fig. 2b.

Atoms			Molecules		
Momentum	Frequency	Decay rate	Momentum	Frequency	Decay rate
$k$	$\Omega/2\pi$ (kHz)	$\eta$ (ms <sup>-1</sup> )	$k$	$\Omega/2\pi$ (kHz)	$\eta$ (ms <sup>-1</sup> )
0	6.77(1)	0.23(1)	0	8.31(1)	0.22(2)
$-2k_L$	6.76(1)	0.19(1)	$-2k_L$	8.30(3)	0.27(4)
$2k_L$	6.78(1)	0.22(2)	$2k_L$	8.35(2)	0.16(6)

TABLE S2. Oscillation frequencies and decay rates of the Bragg diffracted atomic and molecular populations obtained from the fits in Fig. 2d.

Atoms			Molecules		
Momentum	Frequency	Decay rate	Momentum	Frequency	Decay rate
$k$	$\Omega/2\pi$ (kHz)	$\eta$ (ms <sup>-1</sup> )	$k$	$\Omega/2\pi$ (kHz)	$\eta$ (ms <sup>-1</sup> )
0	1.60(1)	0.11(2)	0	2.93(2)	0.15(1)
$2k_L$	1.59(1)	0.10(1)	$2k_L$	2.95(1)	0.14(1)

### C. Phase modulation measurement

We imprint a phase pattern onto the atomic BEC by pulsing on a moving optical lattice with intensity  $I(x, t) = I_0 \sin^2 k_L(x - v_L t)$ , where  $v_L = \hbar k_L/m$  is the recoil velocity of the atom. The lattice potential depth is set to  $3.63(1) E_R$  in all experiments shown in Fig. 3. After the Bragg pulse, we shut off the optical lattice and immediately convert the atoms into molecules in 1.5 ms. Any remaining atoms are blown away with a resonant light pulse. When we blow away the atoms, we simultaneously shut off the DMD potential and let the molecules expand in free space for 16 ms. The dipole trap is left turned on in the  $z$ -direction so the molecules only expand in the  $x$  and  $y$  directions. We dissociate the molecules into atoms at the end of this time-of-flight and image the atoms.

The atomic populations for  $k = 0$  and  $2k_L$  are described by  $n_0 \propto \cos^2 \Omega_a t/2$  and  $n_2 \propto \sin^2 \Omega_a t/2$ , respectively, while the molecular populations for  $k = 0$ ,  $2k_L$  and  $4k_L$  are described by  $m_0 \propto \cos^4 \Omega_0 t/2$ ,  $m_2 \propto \sin^2 \Omega_2 t/2$  and  $m_4 \propto \sin^4 \Omega_4 t/2$ , respectively. A decoherence rate  $\eta$  is added to describe the weak decay in the oscillation amplitudes, shown in Fig. 3c. The results from the fitting are listed in Table S3.

In Fig. 4a, we characterize the phase modulation of the atomic wavefunction  $\phi_a \equiv \phi_a(x = \lambda/4)$  at the anti-nodes of the optical lattice. We extract the phase from the diffracted atomic populations according to

$$\cot^2 \phi_a = \frac{n_0}{n_2}. \quad (\text{S2})$$

When determining the phase beyond the first quadrant ( $0 \leq \phi_a < \pi/2$ ) for Fig. 4a, we use  $\phi_a = \Omega_a t/2$  as a guide to determine the sign of  $\cot \phi_a$  in other quadrants and flip the sign of the cotangent function accordingly. The correct phase in the second quadrant ( $\pi/2 \leq \phi_a < \pi$ ) is given by  $\phi_a = -\cot^{-1} \sqrt{n_0/n_2} + \pi$ . Due to  $\pi$ -periodicity of the cotangent, the third quadrant has the same phase as the first and the fourth has the same as the second, and so on. This operation can be summarized in a single formula as  $\phi_a \pmod{\pi} = (\cot^{-1} \sqrt{n_0/n_2} - \pi/2) \text{sgn}(\sin \Omega_a t) + \pi/2$ , where the function  $\text{sgn}(x) = 1$  for  $x > 0$ , 0 for  $x = 0$  and  $-1$  for  $x < 0$ . We perform a similar operation to get the molecular phase  $\phi_m \pmod{\pi}$ .

Additionally, there is a 1% offset between the measured atomic and molecular Rabi frequencies due to the systematic drift of the lattice beam intensity in the experiment. To compensate for this systematic effect, we apply a correction factor  $\alpha = (\Omega_0 + \Omega_4)/2\Omega_a = 0.987$  to the atomic phase  $\phi_a$  based on the measured Rabi frequencies of the molecules and atoms.

Our determination of both the atomic and molecular phase,  $\phi_a$  and  $\phi_m$ , is sensitive to the variation of the background, which shows a larger systematic uncertainty of the molecular phase near  $\phi_a = 0$  and  $\pi/2$ .

## II. OPTICAL LATTICE CALIBRATION

Dynamics of a particle with mass  $m$  in a one dimensional (1D) lattice potential  $V(x) = V_0 \sin^2 k_L x$  is described by the Schrödinger's equation  $i\hbar \partial_t \psi = H\psi$ , where  $k_L = \pi/d$  is the lattice wavenumber,  $d = \lambda/2$  is the lattice constant.



TABLE S3. Oscillation frequencies and decay rates of the atomic and molecular populations obtained from the fits in Figs. 3c.

Atoms			Molecules		
Momentum	Frequency	Decay rate	Momentum	Frequency	Decay rate
$k$	$\Omega/2\pi$ (kHz)	$\eta$ (ms <sup>-1</sup> )	$k$	$\Omega/2\pi$ (kHz)	$\eta$ (ms <sup>-1</sup> )
0	2.36(1)	0.05(1)	0	2.33(1)	0.08(1)
$2k_L$	2.36(1)	0.03(1)	$2k_L$	4.66(1)	0.03(2)
			$4k_L$	2.33(1)	0.13(2)

The Hamiltonian  $H$  and the solution of the particle's wavefunction  $\psi(x, t)$  are

$$H = -\frac{\hbar^2}{2m}\partial_x^2 + V_0 \sin^2 k_L x. \quad (\text{S3})$$

$$\psi(x, t) = \sum_{j,q} a_{j,q} \phi_{j,q}(x) e^{-iE_{j,q}t/\hbar}. \quad (\text{S4})$$

Here  $E_{j,q}$  is the eigenenergy of the state (dispersion),  $\phi_{j,q}(x)$  is the eigenfunction (Bloch waves),  $j = 0, 1, 2, \dots$  is the Bloch band index,  $-k_L/2 < q < k_L/2$  is the quasi-momentum, and  $a_{j,q}$  is the amplitude. We calculate the eigenstates and the eigenenergies by solving the Mathieu equation

$$(\partial_u^2 + a - 2b \cos 2u)\phi(u) = 0, \quad (\text{S5})$$

where  $a_{j,q} = (E_{j,q} - V_0/2)/E_R$  and  $\phi_{j,q}(u)$  are the characteristic values and functions,  $b = -V_0/4E_R$ ,  $u = kx$ , and  $E_R = \hbar^2 k_L^2 / 2m$  is the recoil energy. The Bloch theorem states that  $\phi_{j,q} = e^{iqx} f_j(x)$ , where  $f_j(x) = f_j(x + d)$  is a periodic function.

### A. Kapitza-Dirac diffraction

Kapitza-Dirac diffraction occurs when the particle is diffracted to multiple quasi-momentum states. When the particle is initially prepared in the zero momentum state  $k = 0$ , the lattice projects the state to different Bloch bands with quasi-momentum  $q = 0$ . The wavefunction is given by

$$\psi(x, t) = \sum_{j=0,2,4,\dots} a_j f_j(x) e^{-iE_{j,0}t/\hbar}, \quad (\text{S6})$$

where  $a_j$  is the amplitude in the  $j$ -th excited band. Only even bands are occupied due to the symmetry of the initial state. In the time-of-flight experiment, the particle is scattered to momentum states  $k_j = \pm j k_L$ .

The Rabi oscillations in the Kapitza-Dirac diffraction experiment, shown in Figs. 2a and 2b, are dominated by the transition of atoms between the ground and second bands at zero quasi-momentum  $q = 0$ , see Fig. S1a, which is given by

$$\hbar\omega_{\text{K.D.}} = E_{2,q=0} - E_{0,q=0}. \quad (\text{S7})$$

### B. Determination of molecular dynamical polarizability

Molecular dynamical polarizability can be determined from molecular response to the optical lattice potential. We measure the atomic and molecular Rabi oscillation frequencies at various lattice beam intensities from Kapitza-Dirac and Bragg diffraction, see Fig. S1. These frequencies provide precise information on the energy dispersion, from which we extract the light shifts induced by the lattice potential. The lattice potential depth is proportional to the lattice intensity,  $V_0 = -\alpha_a I$ , where  $\alpha_a$  is the dynamical polarizability of the atoms in a dipole trap and  $I$  is the lattice intensity. Since the lattice potential depths for atoms and molecules are different despite the lattice intensity being

constant, see examples in Fig. 2b and Fig. S1, this indicates the atomic and molecular polarizabilities are not the same.

We first determine the atomic dynamical polarizability. The light shift on the cesium atoms in the ground state for far-detuned light can be expressed as the weighted sum of the contributions from the  $D_1$  and  $D_2$  lines, which gives [42]

$$V_0 = - \left( f_1 \frac{3\pi c^2}{\omega_1^2} \frac{\Gamma_1}{\omega_1^2 - \omega_0^2} + f_2 \frac{3\pi c^2}{\omega_2^2} \frac{\Gamma_2}{\omega_2^2 - \omega_0^2} \right) I, \quad (\text{S8})$$

where  $f_1 = 1/2.98$  and  $f_2 = 1.98/2.98$  are the line strengths [43],  $\omega_1 = 2\pi \times 335.116$  THz and  $\omega_2 = 2\pi \times 351.726$  THz are the resonant frequencies,  $\Gamma_1 = 2\pi \times 4.56$  MHz and  $\Gamma_2 = 2\pi \times 5.22$  MHz are the natural line widths of the  $D_1$  and  $D_2$  lines, respectively, and  $c$  is the speed of light. Contributions from other higher excited states are negligible.

For lattice beams with wavelength  $\lambda = 1064$  nm, the lattice frequency is  $\omega_0 = 2\pi \times 281.760$  THz, and the atomic polarizability is  $\alpha_a = k_B \times 2.59$  nK  $\cdot$  cm<sup>2</sup>/W. This value allows us to evaluate the intensity of the optical lattice superimposed on the atoms from the measurement of the lattice potential depth.

We compare the lattice potential depths and their corresponding intensities for both atoms and molecules, see Table S4. From the lattice intensity and the induced light shift on the molecules, we determine the molecular polarizability to be  $\alpha_m = k_B \times 5.05(5)$  nK  $\cdot$  cm<sup>2</sup>/W at  $\lambda = 1064$  nm. This is 1.95(2) times greater than the atomic polarizability  $\alpha_a$ . We attribute the slight deviation from the expected ratio of  $\alpha_m/\alpha_a \approx 2$  to the presence of molecular states that Cs<sub>2</sub> molecules can access.

TABLE S4. Atomic and molecular Rabi frequencies and their corresponding lattice potential depths (in units of atomic recoil energy  $E_R$ ) at various lattice intensities shown in Fig. S1.

Lattice intensity (W/mm <sup>2</sup> )	Atoms		Molecules	
	Frequency $\Omega/2\pi$ (kHz)	Lattice depth $V_0$ ( $E_R$ )	Frequency $\Omega/2\pi$ (kHz)	Lattice depth $V_0$ ( $E_R$ )
0.65(1)	5.81(1)	2.65(4)	5.19(2)	5.06(2)
0.92(2)	6.27(3)	3.73(6)	6.70(1)	7.09(2)
1.22(1)	6.92(2)	4.96(4)	8.53(2)	9.64(3)
1.57(1)	7.77(1)	6.37(2)	10.37(4)	12.43(6)
1.96(1)	8.85(2)	7.98(3)	12.16(5)	15.53(9)
2.38(1)	10.06(1)	9.68(2)	13.91(6)	19.03(13)

### C. Bragg diffraction

Bragg diffraction occurs when the particle is resonantly coupled to a single quasi-momentum state. The particle dynamics can be well approximated by coherent Rabi flopping between the initial and the excited states.

In our experiment, Bragg diffraction is realized by imposing an optical lattice  $V(x, t) = V_0 \sin^2 k_L(x - v_L t)$  moving at the recoil velocity  $v_L = \hbar k_L/m$  of the particle. The lattice resonantly excites stationary particles to momentum  $k = 2k_L$  with negligible populations in other states. In the moving frame, the dynamics is described by the same stationary Hamiltonian Eq. (S3) and the particles initially moving with momentum  $-k_L$  in the ground band  $\phi_{0,q=-k_L}$  are driven to  $\phi_{1,q=k_L}$  in the first excited band with momentum  $k_L$ .

The Rabi oscillations in Figs. 2c and 2d are dominated by the transition between the two states. Using  $E_{0,-k_L} = E_{0,k_L}$ , we obtain the Rabi frequency  $\omega_B$  of Bragg scattering as

$$\hbar\omega_B = E_{1,k_L} - E_{0,k_L}. \quad (\text{S9})$$

Bragg scattering induces coherent oscillations between the two states. The wavefunction in the lab frame can be written in the momentum basis, polar form and spin basis as:

$$\psi(x, t) = \cos \tau - i \sin \tau e^{2ik_L x} \quad (\text{S10})$$

$$\equiv \sqrt{n(x, t)} e^{i\phi(x, t)} \quad (\text{S11})$$

$$\equiv e^{-i\hat{\sigma}_x \tau} |0\rangle = \cos \tau |0\rangle - i \sin \tau |2k_L\rangle, \quad (\text{S12})$$

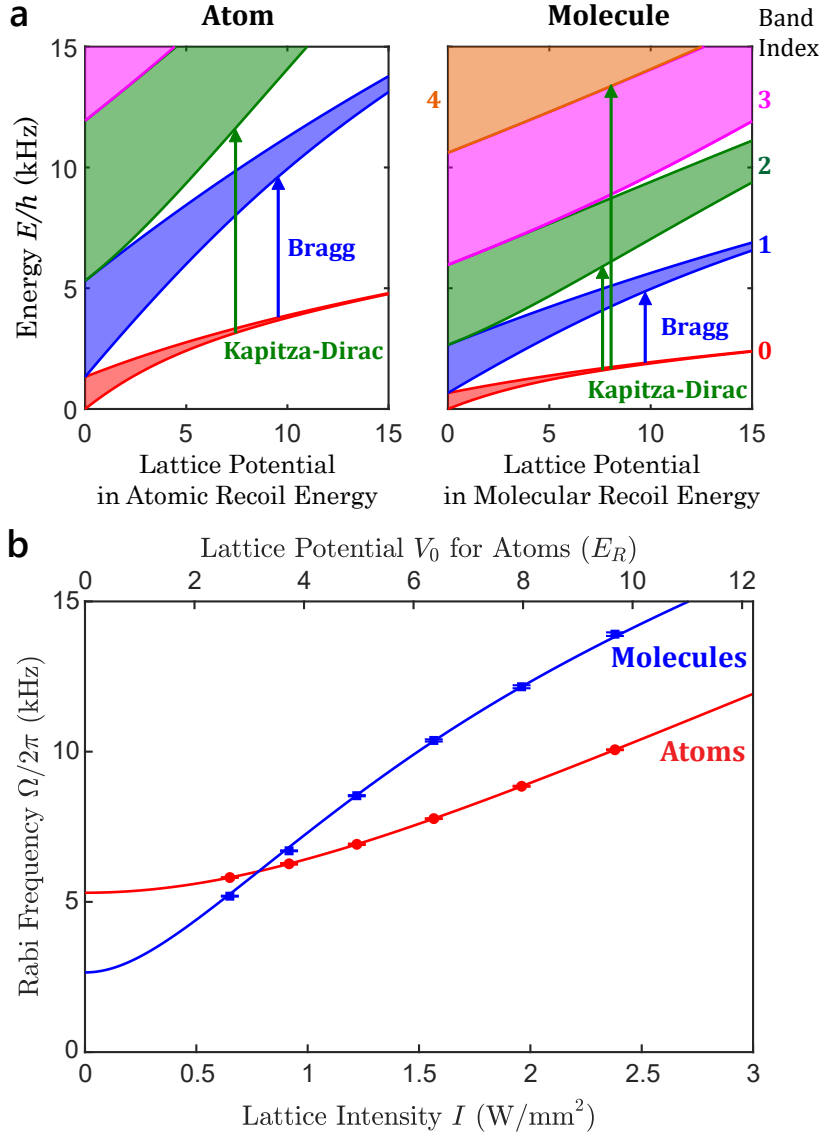


FIG. S1. **Comparison of atomic and molecular polarizabilities.** **a**, Band structure for atoms and molecules in a 1D lattice in units of atomic and molecular recoil energy, respectively. The energies are obtained from the solution of the Mathieu equation. Red, blue, green, magenta and orange filled bands correspond to the ground, 1<sup>st</sup>, 2<sup>nd</sup>, 3<sup>rd</sup> and 4<sup>th</sup> excited bands, respectively. The lower (upper) edge of the red (blue) band corresponds to the energy at quasi-momentum  $q = 0$  while the upper (lower) edge of the red (blue) band corresponds to the energy at  $q = k_L$  and so on for higher excited bands. In our Kapitza-Dirac diffraction experiment, particles are excited from the ground to the 2<sup>nd</sup> excited band at  $q = 0$ . In Bragg diffraction, particles are excited from ground to the 1<sup>st</sup> excited band at  $q = k_L$ . **b**, From the Kapitza-Dirac diffraction measurements, we plot the atomic and molecular Rabi frequencies at various lattice intensities and its corresponding potential depths for atoms (in units of atomic recoil energy  $E_R$ ). The lattice depth is extracted from the Rabi oscillations in which the Rabi frequency corresponds to the energy difference between the ground and 2<sup>nd</sup> excited band. The red solid line is an exact solution to the Mathieu equation for atoms while the blue solid line is a fit based on the solution to the Mathieu equation for molecules with an additional scaling factor to account for the difference in polarizabilities. From fitting the data, we determine the molecular polarizability to be  $\alpha_m = 1.95(2)\alpha_a = k_B \times 5.05(5) \text{ nK} \cdot \text{cm}^2/\text{W}$ , where the atomic polarizability is  $\alpha_a = k_B \times 2.59 \text{ nK} \cdot \text{cm}^2/\text{W}$ .

where  $e^{-i\hat{\sigma}_x\tau}$  is the spin rotation operator that describes the dynamics between the two states  $|k=0\rangle$  and  $|2k_L\rangle$ ,  $\hat{\sigma}_x$  is the Pauli matrix,  $\tau = \Omega t/2$ , and  $n(x,t)$  and  $\phi(x,t)$  are the density and phase of the particle, respectively. The population in the zero-momentum state is  $n_0 = |\langle 0|\psi\rangle|^2 = \cos^2 \tau$  and  $n_2 = |\langle 2k_L|\psi\rangle|^2 = \sin^2 \tau$  in the excited state.

### III. REACTION PHASE $\phi_R = 2\phi_a - \phi_m$

Reactive coupling between atomic and molecular Bose-Einstein condensates can be modeled in the dilute gas limit by two-body Feshbach coupling

$$\hat{H}_2 = \hbar\gamma\hat{\psi}_m^\dagger\hat{\psi}_a^2 + \text{H.c.}, \quad (\text{S13})$$

where  $\gamma$  is the strength of Feshbach coupling,  $\hat{\psi}_m$  and  $\hat{\psi}_a$  are the atomic and molecular field operators, respectively. This Hamiltonian conserves the total particle number  $N_0 = N + 2M$ . In systems with high densities, three-body coupling  $\hat{H}_3 = \hbar\gamma_3\hat{\psi}_m^\dagger\hat{\psi}_a^\dagger\hat{\psi}_a^3 + \text{H.c.}$  dominates [44]. In the following, we consider  $\hat{H}_2$  for simplicity. Generalization of the following calculation to  $\hat{H}_3$  is straightforward.

The equations of motion for the atomic wavefunction  $\hat{\psi}_a$  and the molecular wavefunction  $\hat{\psi}_m$ , and their respective populations  $\hat{N} = \hat{\psi}_a^\dagger\hat{\psi}_a$  and  $\hat{M} = \hat{\psi}_m^\dagger\hat{\psi}_m$  can be obtained from the Heisenberg equation as

$$\partial_t\hat{\psi}_m = -i\gamma\hat{\psi}_a^2 \quad (\text{S14})$$

$$\partial_t\hat{\psi}_a = -2i\gamma\hat{\psi}_a^\dagger\hat{\psi}_m \quad (\text{S15})$$

$$\partial_t\hat{M} = -\frac{1}{2}\partial_t\hat{N} = \frac{i}{\hbar}[\hat{H}_2, \hat{M}] = i\gamma(\hat{\psi}_a^\dagger{}^2\hat{\psi}_m - \hat{\psi}_m^\dagger\hat{\psi}_a^2). \quad (\text{S16})$$

For large atomic populations  $N \equiv \langle\hat{N}\rangle \gg 1$  and molecular populations  $M \equiv \langle\hat{M}\rangle \gg 1$ , we assume both fields are described by coherent states  $|\psi\rangle = |c_a\rangle \otimes |c_m\rangle$ , where  $c_a = \sqrt{N}e^{i\phi_a}$  and  $c_m = \sqrt{M}e^{i\phi_m}$  are complex eigenvalues. The equations of motion for populations  $N$  and  $M$  and the reaction phase  $\phi_R \equiv 2\phi_a - \phi_m$  are given by

$$\begin{aligned} \dot{M} &= -\frac{\dot{N}}{2} \\ &= 2\gamma N\sqrt{M}\sin\phi_R \\ \dot{\phi}_R &= \gamma\frac{N-4M}{\sqrt{M}}\cos\phi_R. \end{aligned}$$

Here we consider a few limiting cases. Atom-molecule equilibrium is reached when atom and molecule numbers are stationary with population  $N = 2N_0/3$  and  $M = N_0/6$ . In this case, the reaction phase is zero  $\phi_R = 0$ , which suggests exact phase doubling.

$$\phi_m = 2\phi_a. \quad (\text{S17})$$

Near equilibrium, we can linearize the equation to leading order in  $\delta M \equiv M - N_0/6$  and  $\delta N \equiv N - 2N_0/3 = -2\delta M$ . The populations and phase oscillate according to

$$\begin{aligned} \delta M(t) &= \delta M(0)\cos\Omega t \\ &= -\frac{1}{2}\delta N(t) = \frac{2N_0^{3/2}}{\sqrt{3}}\phi_R(t), \end{aligned}$$

where the oscillation frequency  $\Omega = \sqrt{8N_0}\gamma$  increases with sample size due to Bose enhancement [44]. This result shows that a positive reaction angle  $\phi_R$  is linked to excess molecules. In addition, the reaction angle near the equilibrium  $\phi_R(t) \propto N_0^{-3/2}\delta M(t)$  approaches zero in the thermodynamic limit  $N_0 \gg 1$ . Thus  $\phi_m \approx 2\phi_a$  remains a very good approximation near equilibrium.

When the system is far from equilibrium, for example, at the beginning of our experiment when the sample is dominated by atoms with  $N \gg 2M \gg 1$ , atoms are paired into molecules. The reaction phase  $\phi_R \approx \pi/2$  is the only stationary solution and the molecular number  $M(t) = (\gamma N_0 t)^2$  increases quadratically with time. Here we have  $2\phi_a = \phi_m + \pi/2$ .

In the opposite limit when the sample is dominated by molecules  $M \gg N/2 \gg 1$ , Feshbach coupling dissociates molecules back to atoms. Here the reaction phase  $\phi_R \approx -\pi/2$  is the only stationary solution and the atom number  $N(t) = N(t)e^{\Omega t}$  increases exponentially due to stimulated reactive dissociation. Thus we have  $2\phi_a = \phi_m - \pi/2$ . We summarize these results in Table S5.



TABLE S5. Summary of the coherent state dynamics of an atom-molecule BEC with resonant Feshbach coupling.

Condition	Atom number $N$	Molecule number $M$	Reaction phase $\phi_R = 2\phi_a - \phi_m$
Equilibrium $N = 4M$	$\frac{2}{3}N_0$	$\frac{1}{6}N_0$	0
Near equilibrium $N \approx 4M$	$\frac{2}{3}N_0 + \Delta \cos \Omega t$	$\frac{1}{6}N_0 - \frac{\Delta}{2} \cos \Omega t$	$\approx 0$
Atom dominated $N \gg 2M$	$\approx N_0$	$(\gamma N_0 t)^2$	$\pi/2$
Molecule dominated $M \gg N/2$	$e^{\Omega t}$	$\approx \frac{1}{2}N_0$	$-\pi/2$

#### IV. MOLECULE SYNTHESIS IN TWO-COMPONENT BECs: COLLECTIVE SPIN PICTURE

When particles are diffracted by a Bragg pulse, it is instructive to represent atoms and molecules in different momentum states using the angular momentum representation. For our experiment in Fig. 3, the full many-body Hamiltonian can be written as

$$H = \sum_{\kappa} \epsilon_{\kappa} (a_{\kappa}^{\dagger} a_{\kappa} + \frac{1}{2} m_{\kappa}^{\dagger} m_{\kappa}) + \hbar \frac{\Omega_a}{2} \sum_{\kappa} (a_{\kappa+2}^{\dagger} a_{\kappa} + a_{\kappa}^{\dagger} a_{\kappa+2}) + \gamma \sum_{\kappa_1, \kappa_2} (m_{\kappa_1+\kappa_2}^{\dagger} a_{\kappa_1} a_{\kappa_2} + \text{H.c.}). \quad (\text{S18})$$

Here we use  $a_{\kappa}^{\dagger}$  and  $a_{\kappa}$  as the atomic field operators,  $m_{\kappa}^{\dagger}$  and  $m_{\kappa}$  are the molecular field operators,  $\kappa_1$  and  $\kappa_2$  are dimensionless momenta in units of the lattice momentum  $k_L$ ,  $\epsilon_{\kappa} = \kappa^2 E_R$  is the kinetic energy of an atom,  $\Omega_a$  is the atomic Rabi frequency induced by the Bragg coupling, and  $\gamma$  is the atom-molecule coupling strength.

The Bragg pulse resonantly couples atoms in two momentum modes  $a_0$  and  $a_2$ , and pairing these atoms produces molecules with 3 modes  $m_0$ ,  $m_2$  and  $m_4$  due to momentum conservation. In the Hilbert space of these modes, we use Schwinger's angular momentum representation to describe the collective excitations of atoms:  $J_x = \frac{1}{2}(a_0^{\dagger} a_2 + a_2^{\dagger} a_0)$ ,  $J_y = \frac{-i}{2}(a_0^{\dagger} a_2 - a_2^{\dagger} a_0)$ ,  $J_z = \frac{1}{2}(a_0^{\dagger} a_0 - a_2^{\dagger} a_2)$ . In the interaction picture, the Hamiltonian reduces to

$$H \equiv -\hbar \Delta m_2^{\dagger} m_2 + \hbar \Omega_a J_x + \hbar \gamma (m_0^{\dagger} a_0^2 + 2m_2^{\dagger} a_0 a_2 + m_4^{\dagger} a_2^2) + \text{H.c.} \quad (\text{S19})$$

In our experiment, the Bragg pulse resonantly couples two atoms with identical momentum  $k$  to a molecule with momentum  $2k$ . However, coupling two atoms with momenta 0 and  $2k_L$  into a molecule, described by  $m_2^{\dagger} a_0 a_2$ , is an off-resonant process with detuning  $\hbar \Delta = 2E_R$  since the molecule with  $2k_L$  has a lower kinetic energy than the atoms by two atomic recoil energies  $2E_R$ . This detuning is included in the first term of the Hamiltonian.

Atoms are initially prepared in the BEC with zero momentum  $k = 0$ , collectively described by  $|i\rangle \equiv |J = N/2, m_J = -J\rangle$ . The Bragg pulse rotates the state by  $R = e^{-i\Omega_a t J_x}$ . The pulse is followed by the Feshbach coupling  $\gamma$ , which pairs the atoms into molecules in three different momentum modes. From the Heisenberg picture, the equation of motion and the production of molecules in different states at very short times are given by

$$i\partial_t m_0 = -[H, m_0] = \gamma a_0^2 \Rightarrow M_0 \approx \langle a_0^{\dagger} a_0^{\dagger} a_0 a_0 \rangle \gamma^2 t^2 = N_0(N_0 - 1) \gamma^2 t^2 \quad (\text{S20})$$

$$i\partial_t m_2 = -[H, m_2] = -\Delta m_2 + 2\gamma a_0 a_2 \Rightarrow M_2 \approx 4 \langle a_0^{\dagger} a_2^{\dagger} a_2 a_0 \rangle \gamma'^2 t^2 = 4N_0 N_2 \gamma_2'^2 t^2 \quad (\text{S21})$$

$$i\partial_t m_4 = -[H, m_4] = \gamma a_2^2 \Rightarrow M_4 \approx \langle a_2^{\dagger} a_2^{\dagger} a_2 a_2 \rangle \gamma^2 t^2 = N_2(N_2 - 1) \gamma^2 t^2, \quad (\text{S22})$$

where  $N_0 = \langle a_0^{\dagger} a_0 \rangle$  and  $N_2 = \langle a_2^{\dagger} a_2 \rangle$  are the atomic populations in  $k = 0$  and  $2k_L$  modes, and  $M_0 \equiv \langle m_0^{\dagger} m_0 \rangle$ ,  $M_2 \equiv \langle m_2^{\dagger} m_2 \rangle$  and  $M_4 \equiv \langle m_4^{\dagger} m_4 \rangle$  are the molecular populations in  $k = 0$ ,  $2k_L$ , and  $4k_L$  modes, and  $\gamma_2 = \sqrt{g^{(2)}} \gamma'$  is the off-resonance atom-molecule coupling. We introduce the second order correlation function to factorize the correlation of the atomic fields as

$$g^{(2)} = \frac{\langle a_0^{\dagger} a_2^{\dagger} a_2 a_0 \rangle}{\langle a_0^{\dagger} a_0 \rangle \langle a_2^{\dagger} a_2 \rangle}. \quad (\text{S23})$$

For Bragg-diffracted atomic BEC, we expect the correlation function to be  $g^{(2)} = (N - 1)/N \approx 1$ , where  $N \gg 1$  is the atom number.

## V. MOLECULE SYNTHESIS OF DIFFRACTED ATOMS: MEAN-FIELD PICTURE

To compare our measurement results with theory, we model the atomic and molecular wavefunctions based on mean-field wavefunctions. Given the wavefunction of a Bragg-diffracted atom is  $\psi_a(x) \equiv \psi_{a0} + \psi_{a2}e^{2ik_Lx} = \cos\tau - i\sin\tau e^{2ik_Lx}$ , where  $\tau = \Omega_a t/2$  and the molecular wavefunction is  $\psi_m(x) \equiv \psi_{m0} + \psi_{m2}e^{2ik_Lx} + \psi_{m4}e^{4ik_Lx}$ . The result of Eq. (20-22) can be translated into the probabilities to find the molecule in the 3 momentum modes, which give

$$m_0 = |\psi_{m0}|^2 \propto \gamma^2 |\psi_{a0}|^4 = \gamma^2 \cos^4 \tau \quad (\text{S24})$$

$$m_2 = |\psi_{m2}|^2 \propto 4\gamma_2^2 |\psi_{a0}|^2 |\psi_{a2}|^2 = \gamma_2^2 \sin^2 2\tau \quad (\text{S25})$$

$$m_4 = |\psi_{m4}|^2 \propto \gamma^2 |\psi_{a4}|^4 = \gamma^2 \sin^4 \tau. \quad (\text{S26})$$

These are the fit functions we used in Fig. 3b to describe the molecular data. Based on the equations above, we model the molecular wavefunction as

$$\psi_m(x, t) \equiv \langle x | \psi_m \rangle = A_m (\gamma \cos^2 \tau - 2i\gamma_2 \sin \tau \cos \tau e^{2ik_Lx} - \gamma \sin^2 \tau e^{4ik_Lx}) \quad (\text{S27})$$

$$\equiv \sqrt{m(x, t)} e^{i\phi_m(x, t)}, \quad (\text{S28})$$

where  $A_m = [\gamma^2 + (\gamma_2^2 - \gamma^2/2) \sin^2 2\tau]^{-1/2}$  is the normalization constant. Here we have introduced the density  $m(x, t)$  and phase  $\phi_m(x, t)$  of the molecular wavefunction. The probabilities of molecules with momenta 0,  $2k_L$  and  $4k_L$  are

$$m_0 = A_m^2 \gamma^2 \cos^4 \tau \quad (\text{S29})$$

$$m_2 = A_m^2 \gamma_2^2 \sin^2 2\tau \quad (\text{S30})$$

$$m_4 = A_m^2 \gamma^2 \sin^4 \tau. \quad (\text{S31})$$

In particular, the maximum population of  $m_2(\tau = \pi/4) = \gamma_2^2/(\gamma_2^2 + \gamma^2/2)$  is reached after a  $\pi/2$ -pulse on the atoms. From the measurement of  $m_2 = 0.58(1)$ , we determine  $\gamma_2/\gamma = 0.82(3)$ . The smaller value of sum-frequency coupling constant  $\gamma_2$  compared to Feshbach coupling  $\gamma$  can indicate anti-correlations between the populations in  $k = 0$  and  $2k_L$  modes. In addition, the detuning of the sum-frequency process  $\delta E = -2E_R = -h \times 2.7$  kHz is not negligible compared to the coupling strength  $\Gamma = \delta\mu\Delta B = h \times 6.3(5)$  kHz of the  $g$ -wave Feshbach resonance, calculated from the resonance width  $\Delta B = 8.3(5)$  mG and relative magnetic moment  $\delta\mu = h \times 0.76(3)$  MHz/G [31]. The atom-molecule conversion efficiency for the sum-frequency process is thus suppressed. Using the Lorentzian lineshape as an estimation, we obtain a lower conversion efficiency of  $1/(1 + 4\delta E^2/\Gamma^2) \approx 0.59(4)$ , leading to  $\gamma_2/\gamma = \sqrt{0.59(4)} = 0.77(3)$ , which is consistent with our observed value  $\gamma_2/\gamma = 0.82(3)$ .

The phase modulation of the molecular wavefunction evaluated at the anti-nodes of the optical lattice  $\phi_m \equiv \phi_m(x = \lambda/4)$  gives

$$\phi_m = \cot^{-1} \frac{\sqrt{m_0} - \sqrt{m_4}}{\sqrt{m_2}} = \cot^{-1} \frac{\gamma}{\gamma_2} \cot 2\tau. \quad (\text{S32})$$

We may express the molecular phase  $\phi_m$  in terms of the atomic phase  $\phi_a = \tau$  using Eq. (S32), which gives

$$\phi_m = \cot^{-1} \frac{\gamma}{\gamma_2} \cot 2\phi_a \quad (\text{S33})$$

$$= 2\phi_a - \epsilon \sin 4\phi_a + \mathcal{O}(\epsilon^2), \quad (\text{S34})$$

where we have expanded the nonlinear parameter  $\epsilon = (1 - \gamma_2/\gamma)/2$  to leading order. This expression shows that the perfect phase doubling  $\phi_m = 2\phi_a$  occurs when the atom-molecule coupling is momentum insensitive  $\gamma_2 = \gamma$  and the correlator is  $g^{(2)} = 1$ .

## VI. PARITY, COHERENCE AND ENTANGLEMENT OF THE MOLECULAR STATE

Consider  $N$  spins with angular momenta  $\vec{s}_j = \frac{\hbar}{2}\vec{\sigma}_j$  for the  $j$ -th spin, where  $\vec{\sigma}$  is the Pauli vector. We define the spin coherence operators as  $\hat{C}_{kk} = \prod_j^N \sigma_{j,k}$ , where  $k = x, y$  and  $z$ .

For  $N = 2$  spins in a product state  $|\psi\rangle = |1\rangle \otimes |2\rangle$ , for instance, we can define the Bloch vectors  $\vec{b}_j = \langle j|\vec{\sigma}|j\rangle = (b_{j,x}, b_{j,y}, b_{j,z})$ , where  $j = 1, 2$  refers to the spins and  $|\vec{b}_j| = 1$ . The combinations of the correlators for any product state are bound as

$$\pm C_{xx} \pm C_{yy} \pm C_{zz} \leq |C_{xx}| + |C_{yy}| + |C_{zz}| \quad (\text{S35})$$

$$|C_{xx}| + |C_{yy}| + |C_{zz}| = |\langle\psi|\sigma_{1,x}\sigma_{2,x}|\psi\rangle| + |\langle\psi|\sigma_{1,y}\sigma_{2,y}|\psi\rangle| + |\langle\psi|\sigma_{1,z}\sigma_{2,z}|\psi\rangle| \quad (\text{S36})$$

$$= |b_{1,x}b_{2,x}| + |b_{1,y}b_{2,y}| + |b_{1,z}b_{2,z}| \quad (\text{S37})$$

$$\leq \sqrt{b_{1,x}^2 + b_{1,y}^2 + b_{1,z}^2} \sqrt{b_{2,x}^2 + b_{2,y}^2 + b_{2,z}^2} = 1. \quad (\text{S38})$$

In our experiment, two atoms are paired into a molecule. If the molecular state is a product state of the atoms with identical Bloch vectors  $\vec{b}_1 = \vec{b}_2 = (b_x, b_y, b_z)$ , the parity  $C_{zz}$  is constrained as

$$C_{zz} = \langle\psi|\sigma_{1,z}\sigma_{2,z}|\psi\rangle = b_z^2 \quad (\text{S39})$$

$$0 \leq b_z^2 \leq b_x^2 + b_y^2 + b_z^2 = 1 \quad (\text{S40})$$

$$\Rightarrow 0 \leq C_{zz} \leq 1. \quad (\text{S41})$$

Thus our measurement of parity covering a range  $-0.15 \lesssim C_{zz} < 1$  indicates that the molecular state is not a product state of two atoms. The strongest violation occurs when the atoms are prepared in the equal superposition state of  $|0\rangle$  and  $|2k_L\rangle$  after the  $\pi/2$  pulse.

For an entangled state, the above inequality Eq. (S41) can be violated. For example, for Bell states  $\Psi^\pm = (|0,0\rangle \pm |1,1\rangle)/\sqrt{2}$  and  $\Phi^\pm = (|0,1\rangle \pm |1,0\rangle)/\sqrt{2}$ , the combinations  $\hat{W}_{\Psi^\pm} = \pm\hat{C}_{xx} \mp \hat{C}_{yy} + \hat{C}_{zz} - \hat{1}$  and  $\hat{W}_{\Phi^\pm} = \pm\hat{C}_{xx} \pm \hat{C}_{yy} - \hat{C}_{zz} - \hat{1}$  serve as entanglement witnesses, which are greater than zero for the corresponding Bell states

$$\langle\Psi^\pm|\hat{W}_{\Psi^\pm}|\Psi^\pm\rangle = \langle\Phi^\pm|\hat{W}_{\Phi^\pm}|\Phi^\pm\rangle = 2. \quad (\text{S42})$$

For product states, on the other hand, the witnesses give nonpositive values  $W_{\Psi^\pm}, W_{\Phi^\pm} \leq 0$ . Possible witness values are summarized in Table S6.

TABLE S6. Bell state witnesses for different two-spin states. The last column shows the expected witnesses for the ideal case when Feshbach couplings for sum frequency and second harmonic generation are equal.

	$ \Psi^+\rangle = \frac{ 00\rangle+ 11\rangle}{\sqrt{2}}$	$ \Psi^-\rangle = \frac{ 00\rangle- 11\rangle}{\sqrt{2}}$	$ \Phi^+\rangle = \frac{ 01\rangle+ 10\rangle}{\sqrt{2}}$	$ \Phi^-\rangle = \frac{ 01\rangle- 10\rangle}{\sqrt{2}}$	product state	our molecules after $\tau = \pi/4$	$\gamma_2 = \gamma$
$W_{\Psi^+}$	2	-2	-2	-2	$\leq 0$	<b>-2</b>	-2
$W_{\Psi^-}$	-2	2	-2	-2	$\leq 0$	<b>-0.23(2)</b>	-2/3
$W_{\Phi^+}$	-2	-2	2	-2	$\leq 0$	<b>0.29(2)</b>	2/3
$W_{\Phi^-}$	-2	-2	-2	2	$\leq 0$	<b>-2</b>	-2

We may evaluate the witnesses for the molecular wavefunction in Eqs. (S27-S31), which gives

$$C_{xx} = m_2 - 2\sqrt{m_0 m_4} \quad (\text{S43})$$

$$C_{yy} = m_2 + 2\sqrt{m_0 m_4} \quad (\text{S44})$$

$$C_{zz} = m_0 - m_2 + m_4 \quad (\text{S45})$$

$$W_{\Phi^+} = 3m_2 - m_0 - m_4 - 1 = -2C_{zz} \quad (\text{S46})$$

$$W_{\Phi^-} = -m_0 - m_2 - m_4 - 1 = -2 \quad (\text{S47})$$

$$W_{\Psi^+} = m_0 - m_2 + m_4 - 4\sqrt{m_0 m_4} - 1 \quad (\text{S48})$$

$$W_{\Psi^-} = m_0 - m_2 + m_4 + 4\sqrt{m_0 m_4} - 1. \quad (\text{S49})$$

In our experiment, after  $\pi/2$  pulse on the atoms we observe  $m_2 = 0.58(1)$  and  $m_0 = m_4 = 0.21(1)$  on the molecules. We evaluate the entanglement witness  $W_{\Phi^+}$  using Eq. (S46). From fitting the witness with Eqs. (S29-S31) and Eqs. (S46-S49), with amplitude and frequency as free parameters, we obtain  $W_{\Phi^+} = 0.29(2)$  at  $\tau = \pi/4, 3\pi/4, \dots$ ,

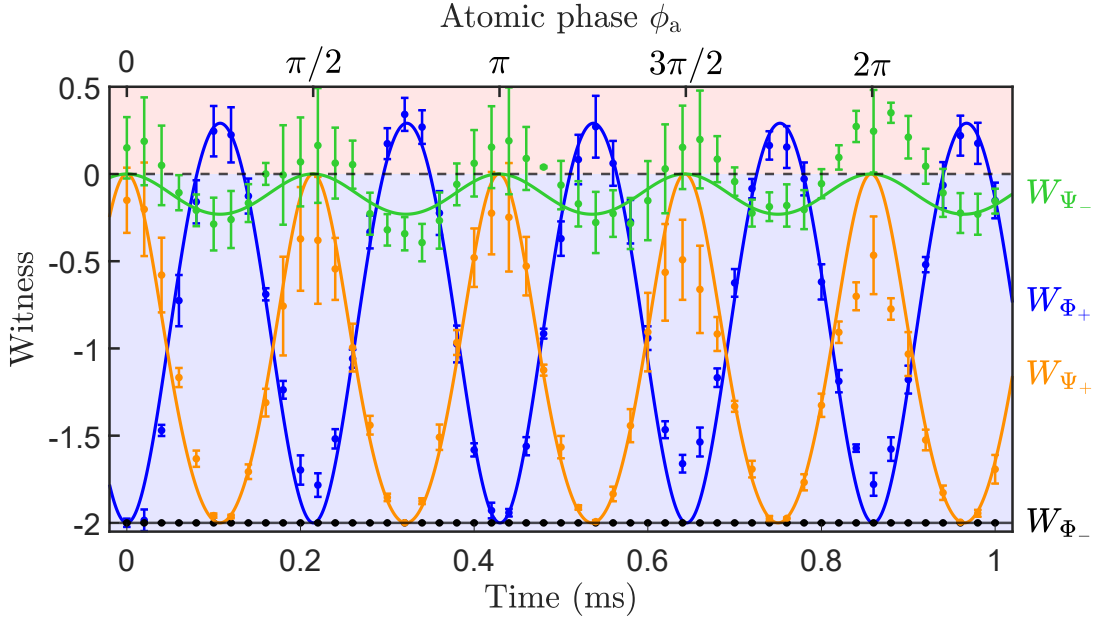


FIG. S2. **Entanglement witnesses.** We plot  $W_{\Psi+}$  (orange),  $W_{\Psi-}$  (green),  $W_{\Phi+}$  (blue), and  $W_{\Phi-}$  (black) as a function of time  $t$ . The red and blue areas represent non-separable and separable states, respectively.  $W_{\Phi+}$  exceeds the upper limit of zero at  $\phi_a = \pi/4, 3\pi/4, 5\pi/4, 7\pi/4, \dots$ , reaching a maximum of  $W_{\Phi+} = 0.29(2)$  from the fit, thus indicating entanglement.  $W_{\Psi-}$  appears to exceed zero at  $\phi_a = 0, \pi/2, \pi, 3\pi/2, \dots$ , due to large relative uncertainties of the populations close to zero in Eq. (S49). However, most atoms are in a single momentum state (either  $|0\rangle$  or  $|2k_L\rangle$ ) at  $\phi_a = 0, \pi/2, \pi, 3\pi/2, \dots$  and thus are unable to generate an entangled state.

which suggests the molecular state is not a separable state and is more aligned with  $\Phi^+$  than with all other states with lower values of  $W_{\Phi-} = -2$ ,  $W_{\Psi+} = -2$  and  $W_{\Psi-} = -0.23(2)$ .

For a  $\pi/2$ -pulse, the witness  $W_{\Phi+}$  from Eq. (S46) can be expressed in terms of ratio  $\gamma_2/\gamma$  as

$$W_{\Phi+}(\tau = \pi/4) = \frac{2\gamma_2^2 - \gamma^2}{\gamma_2^2 + \gamma^2/2}. \quad (\text{S50})$$

By using Eqs. (S27-S31), Eq. S46 and  $m_0(\tau = \pi/4) = m_4(\tau = \pi/4)$ , we can express the molecular wavefunction after  $\pi/2$ -pulse as

$$|\psi_m(\tau = \pi/4)\rangle = \frac{1}{2}\sqrt{2 - W_{\Phi+}}|\Psi^-\rangle - \frac{i}{2}\sqrt{2 + W_{\Phi+}}|\Phi^+\rangle. \quad (\text{S51})$$